Near-Wall μ-PIV Reveals a Hydrodynamically Relevant Endothelial Surface Layer in Venules In Vivo

Michael L. Smith,* David S. Long,† Edward R. Damiano,† and Klaus Ley*‡

*Department of Biomedical Engineering and ‡Cardiovascular Research Center, University of Virginia Health Science Center, Charlottesville, Virginia 22908; and †Department of Mechanical and Industrial Engineering, University of Illinois at Urbana-Champaign, Urbana, Illinois 61801

ABSTRACT High-resolution near-wall fluorescent microparticle image velocimetry (μ-PIV) was used in mouse cremaster muscle venules in vivo to measure velocity profiles in the red cell-depleted plasma layer near the endothelial lining. μ-PIV data of the instantaneous translational speeds and radial positions of fluorescently labeled microspheres (0.47 μm) in an optical section through the midsagittal plane of each vessel were used to determine fluid particle translational speeds. Regression of a linear velocity distribution based on near-wall fluid-particle speeds consistently revealed a negative intercept when extrapolated to the vessel wall. Based on a detailed three-dimensional analysis of the local fluid dynamics, we estimate a mean effective thickness of ~0.33 μm for an impermeable endothelial surface layer or ~0.44 μm assuming the lowest hydraulic resistivity of the layer that is consistent with the observed particle motions. The extent of plasma flow retardation through the layer required to be consistent with our μ-PIV data results in near complete attenuation of fluid shear stress on the endothelial-cell surface. These findings confirm the presence of a hydrodynamically effective endothelial surface layer, and emphasize the need to revise previous concepts of leukocyte adhesion, stress transmission to vascular endothelium, permeability, and mechanotransduction mechanisms.

INTRODUCTION

The interface between blood and the vascular endothelium is complex, dynamic, and fundamentally important in mammalian physiology. Strategically located at this interface is a glycocalyx surface layer, which is regulated by and expressed on vascular endothelial cells. The glycocalyx is a layer of membrane-bound macromolecules (Pries et al., 2000) with a thickness estimated from electron microscopy studies to be ~100 nm (Haldenby et al., 1994; Sims and Horne, 1994). This estimate, however, is likely to fall considerably short of the true in vivo dimension of the layer since significant dehydration of the extracellular matrix inevitably accompanies tissue fixation in all of these studies.

Visual evidence for the existence of an endothelial surface layer (ESL) in vivo was first provided by the exclusion of plasma-borne fluorescein-5-isothiocyanate-dextran (FITC-dx) in capillaries and small postcapillary venules (<15 μm in diameter) (Vink and Duling, 1996; Henry and Duling, 1999). Using intravital microscopy, these studies showed that 70 kDa dextran molecules were sterically excluded from a region ~0.4–0.5 μm in thickness adjacent to the endothelial-cell surface. Indirect evidence that the ESL has an influence on vascular resistance in small vessels <30 μm in diameter was provided by the observation that flow resistance decreased in microvascular networks (Pries et al., 1997) after infusion of heparinase, an enzyme that appears to partially degrade the ESL (Desjardins and Duling, 1990; Henry and Duling, 1999).

The ability of the ESL to exclude large dextran molecules and limit the cross-sectional area available to red cells passing through capillaries suggests that it might be an important determinant of microfluidics near the vessel wall. This was first suggested on theoretical grounds by considering the pressure-driven flow of a fluid suspension of rigid spheres in a tube lined with a porous layer (Damiano et al., 1996) and by models of single-file red-cell motion in glycocalyx-lined capillaries (Damiano, 1998b; Secomb et al., 1998). These studies all assumed that the hydraulic permeability of the glycocalyx to plasma was quite low. Using an estimate of glycocalyx fixed-charge density, based on a recent electrochemical model of the glycocalyx (Stace and Damiano, 2001), Damiano and Stace (2002) were able to estimate the hydraulic resistivity of the ESL (which is inversely proportional to its hydraulic permeability) from their mechano-electrochemical model of the layer to be between 10^{10} and 10^{11} dyn-s/cm^4. This is consistent with an earlier estimate by Feng and Weinbaum (2000), which was inferred from a fiber matrix model of the glycocalyx based on the Brinkman equation.

In addition to impeding blood flow, recent studies suggest that the ESL might play an important role in modulating inflammation. A modeling study explored the potential role of the ESL in interfering with leukocyte tethering to vascular endothelium and thereby inhibiting the leukocyte adhesion cascade. The model suggests that the glycocalyx prevents leukocyte microvilli penetration and tethering when shear stress near the vessel wall exceeds ~2 dyn/cm^2 (Zhao et al., 2001). Direct evidence for a change in the structure of the glycocalyx during inflammation was provided by Henry and

Submitted January 27, 2003, and accepted for publication March 21, 2003.

Address reprint requests to Klaus Ley, M.D., Dept. of Biomedical Engineering, University of Virginia Health Science Center, PO Box 800759, Charlottesville, VA 22908. Tel.: 434-243-9966; Fax: 434-982-3870; E-mail: klausley@virginia.edu.

0006-3495/03/07/637/09 $2.00

Duling (2000), who showed that the width of the FITC-dx exclusion zone was decreased in hamster cremaster microvessels after exposure to tumor necrosis factor-α. A recent study reported that the adhesion of microspheres coated with an antibody to ICAM-1 increased significantly after manipulation aimed at degrading the glycocalyx (Mulivor and Lipowsky, 2002). These studies suggest that glycocalyx degradation may be an important regulator of leukocyte adhesion.

Using dual-flash epi-illumination of fluorescent microspheres, intravital microparticle image velocimetry (μ-PIV) was used to estimate fluid velocity profiles in the near-wall plasma-rich region of venules before and after light-dye treatment to degrade the ESL. The resulting velocity profiles are indicative of a hydrodynamically relevant surface layer, with a thickness that is comparable to earlier estimates based on dye-exclusion techniques, and provide the first direct evidence that the layer significantly impedes fluid flow near the vessel wall in postcapillary venules in vivo.

MATERIALS AND METHODS

Animals

All animal experiments were conducted under a protocol approved by the University of Virginia institutional animal care and use committee (Protocol No. 2474). Wild-type (WT) male mice (C57Bl/6) were obtained from Hilltop Labs (Scottsdale, PA). Tie2 green fluorescent protein (GFP) transgenic mice were obtained from established colonies derived from founders as described (Motoike et al., 2000). All transgenic mice used in this study were offspring of F2 intercrosses. All mice appeared healthy and were between 8 and 14 weeks of age.

Intravital microscopy

Mice were anesthetized with an intraperitoneal injection of ketamine (125 mg/g body weight, Ketalar; Parke-Davis, Morris Plains, NJ), xylazine (12.5 mg/g body weight; Phoenix Scientific, St. Joseph, MO), and atropin sulfate (0.025 mg/g body weight; Elkins-Sinn, Cherry Hill, NJ) and placed on a 38°C heating pad. The trachea was intubated using polyethylene 90 tubing (Becton Dickinson, Sparks, MD) to allow spontaneous respiration. The left carotid artery was cannulated using polyethylene 10 tubing. The carotid cannula was needed for administration of additional anesthetic, microspheres, FITC-dextran, blood pressure monitoring, and the withdrawal of blood samples.

The cremaster muscle was prepared for intravital microscopy as described (Baez, 1973; Ley et al., 1995). The cremaster was exteriorized, pinned to the stage, and superfused with thermocontrolled bicarbonate-buffered saline (131.9 mM NaCl, 18 mM $NaHCO_3$, 4.7 mM KCl, 2.0 mM $CaCl_2{\cdot}2H_2O$, and 1.2 mM $MgCl_2$) equilibrated with 5% CO_2 in N_2. This procedure was completed in 6–10 min.

Intravital fluorescent μ-PIV

Microscopic observations were made on a Zeiss intravital microscope (Axioskop, Carl Zeiss, Thornwood, NY) with a X100 saline immersion objective (NA 1.0). Venules 24–41 μm diameter with clear focus at least 5 diameters from the nearest upstream bifurcation were selected for intravital microscopy. Neutrally buoyant Fluoresbrite YG Microspheres (0.47 ± 0.01 μm, $\rho = 1.05$ g/cm^3, Polysciences, Warrington, PA) were washed twice in isotonic saline with 1% bovine serum albumin and resuspended in saline. A small volume of microspheres (<0.03 ml) was slowly injected through the carotid cannula until 10–20 beads per s passed through the vessel. This concentration was optimal for velocity measurements. All measurements were obtained within 10 s per venule to reduce the impact of possible changes in blood volume flow rate. The microspheres were visualized using stroboscopic double-flash (5–16.67 ms apart, Strobex 11360, Chadwick Helmuth, Mountain View, CA) epi-illumination, and recordings were made through a CCD camera (model VE-1000CD, Dage-MTI, Michigan City, IN) on a Panasonic S-VHS recorder. This technique yields, in one picture, two images of the same microsphere displaced a measurable distance over a known time interval. Transillumination was maintained to keep the vessel wall clearly visible. The midsagittal plane of each venule was defined as the point at which the contrast of the edge of the intraluminal wall reversed (Gretz and Duling, 1995). Carotid blood pressure measurements (model AH 60-3002, Harvard Apparatus, Holliston, MA) were taken intermittently during each experiment.

Light-dye modification of ESL

Based on a method published earlier (Vink and Duling, 1996), FITC-dx 70 (Sigma Chemical St. Louis, MO) in 0.9% saline was slowly infused through the carotid cannula (~0.05 mL, 20 mg/mL) until the venular lumen was sufficiently bright without obscuring visualization of fluorescent microspheres. After 10 min, the cremaster muscle was continuously epi-illuminated for 5 min at 450–490 nm with a mercury vapor short-arc lamp (50 W, HBO 50, Carl Zeiss) and a X20 (saline immersion, NA 0.50) objective to degrade the ESL (Vink and Duling, 1996). Microsphere velocity recordings were then made as described above using the X100 objective.

Measurement of brightfield and fluorescent diameters

Randomly selected capillaries and venules were recorded with the X100 objective during either transillumination or epi-illumination in Tie2-GFP transgenic mice or WT mice after infusion of FITC-dx. The location of the endothelial membrane under brightfield illumination was determined as described (Gretz and Duling, 1995). As one focuses through the midsagittal plane of the vessel, the contrast of the intraluminal wall reverses and only a dark band (of finite thickness ranging between 0.1 and 0.5 μm) remains. This focal plane is taken to correspond to the midsagittal plane of the vessel. The brightfield endothelial surface was defined as the luminal edge of this dark band. In most cases, the edge of the endothelial surface appeared to transition from dark to light (the shade of the rest of the plasma-rich zone) over only two pixels. In such a case, the light pixel was used to define the edge of the endothelium. If the edge of the endothelium appeared across three pixels, with the middle pixel possessing an intermediate light intensity, the middle pixel was considered the edge of the endothelium. This approach was objectively and consistently applied to each vessel. The brightfield diameter was taken to be the distance between the luminal edges of these two dark bands. Similarly, two fluorescent bands appeared in the Tie2-GFP mouse and the diameter was taken to be the distance between the luminal edges of these two fluorescent bands. Epi-illumination was performed using strobe illumination to reduce endothelial damage. These measurements were also made in WT vessels after continuous epi-illumination in the presence of FITC-dx to degrade the ESL as described above.

Erythrocyte dimensions

To assess the impact of possible optical artifacts, arising from differences in the refractive indices of plasma and surrounding tissue, we measured the length of radially or axially aligned erythrocytes in venules between 10 and 14 μm in diameter that were occluded with a blunt micropipette.

Micropipettes were drawn to a tip diameter of ~10 μm and flamed to produce a curved, blunt tip (Micropipette Puller, Stoelting, Wood Dale, IL). Flow cessation in the vessels was achieved by occlusion using a micromanipulator (Model MMN-333, Narishige, McHenry, IL). Axially aligned erythrocytes were defined as those that were aligned with their symmetry axis perpendicular to the vessel axis (limited to within $\pm 5°$) but parallel with the microscope's focal plane, whereas radially aligned erythrocytes were defined as cells with their symmetry axis aligned parallel to the vessel axis (limited to within $\pm 25°$) and parallel to the focal plane. A difference in the refractive indices of plasma and the surrounding tissue would result in a systematic difference in the apparent width of axially and radially aligned erythrocytes. Cells that appeared to touch other erythrocytes, leukocytes, or the endothelium were excluded. Intermittent flow cessation was allowed until erythrocytes that met these criteria could be recorded.

In addition, measurements of axially and radially aligned erythrocytes were made in vitro to confirm the presence of a known optical artifact resulting from the difference in refractive indices of glass and plasma. The in vitro perfusion system (Reinke et al., 1987) was made of glass capillary tubes (length 2.5 cm, ID 31.9 μm) mounted horizontally on a microscope stage. Diameters were determined by end-on microscopy. Capillaries were immersed in phthalic acid ($ND = 1.48$, Sigma), which has an index of refraction that effectively eliminates optical refraction at the outer wall. The upstream end of the glass capillary was placed in the perfusion fluid, and the downstream end was attached via silastic tubing (Dow Corning, Midland, MI) to a reservoir that could be manipulated vertically with a vernier caliper (Nolan Supply, Syracuse, NY). The system was filled with degassed saline before the withdrawal of the erythrocyte solution from the upstream reservoir. The pressure head was manipulated to first draw erythrocytes into the field of view and then stop the flow. This procedure was repeated until sufficient numbers of erythrocytes were measured. Recordings were made as described above using a saline immersion X63 objective (NA 0.90) under brightfield illumination. Blood was obtained from wild-type mice by heart puncture, and the buffy coat was removed from centrifuged samples (600 g for 10 min). Erythrocytes were reconstituted in plasma at a hematocrit of ~2% measured using a Hemavet 850 (CDC Technologies, Oxford, CT). The refractive index of plasma, ND_p, was measured using a hand refractometer (Atago, Kirkland, WA). Snell's law was used to predict the observed decrease in the length of radially aligned erythrocytes. Assuming the erythrocyte is located in the midsagittal plane of the capillary and the cross section is circular, Snell's law predicts that

$$ND_g \sin\theta_1 = ND_p \sin\theta_2, \tag{1}$$

where ND_g is the refractive index of glass (~1.48), θ_1 is the angle of incidence, and θ_2 is the angle of refraction. Based on purely geometric arguments, one can use Eq. 1 to show that in a cylindrical tube of radius R, the actual distance from the tube wall, d_a, to the edge of an erythrocyte is related to the observed (i.e., measured) distance, d_m, according to

$$d_a = d_m - \delta x, \tag{2}$$

where

$$\delta x = \sqrt{d_m(2R - d_m)}\tan\left[\sin^{-1}\left(\frac{ND_g}{ND_p}\sin\theta_1\right) - \theta_1\right] \tag{3}$$

and

$$\theta_1 = \frac{\pi}{2} - \tan^{-1}\left(\frac{d_m(2R - d_m)}{R - d_m}\right).$$

The actual distance of the edge of an erythrocyte from the tube wall was predicted using Eq. 2 where the error, δx, in using the measured distance for the actual distance is strictly positive since $ND_g > ND_p$. Thus, in glass tubes, the actual position of an object is closer to the tube wall than it would appear based on its observed position, and this thereby decreases the apparent length of radially relative to axially aligned erythrocytes.

Data analysis

A MicroMotion DC30 video compression card (Pinnacle Systems, Mountain View, CA) was used to digitize video recordings from a JVC HR-53600U VHS recorder into a Macintosh computer (Adobe Premiere software). Digitized video clips were analyzed with the public domain NIH Image program (http://rsb.info.nih.gov/nih-image/). All analysis was performed using custom-written macros similar to ones previously described (Norman, 2001). Vessel diameter was determined as the average of three measurements for each vessel. The diameter of the Tie2-GFP vessels, FITC-dx columns, and radially or axially aligned erythrocytes were measured in a similar manner. The fluorescent exclusion zone was defined as one-half of the difference in brightfield and FITC-dx fluorescent diameters.

Abbe's equation was used to predict a theoretical maximum resolution corresponding to the minimum measurable distance (0.31 μm for light having a 500 nm wavelength) between two distinct objects that can be discretely resolved (Inoue, 1986). The final calibration, using a video image of a 0.01 mm objective micrometer slide after digitization and import into NIH Image, was 5.43 pixels/μm.

For microsphere velocity measurements, the flash-time interval was chosen such that the two images for a given microsphere were 3–10 μm apart. All microspheres appeared as a double image, and neither very fast nor very slow beads were missed. The distance between these two images, and the shortest distance between the microsphere center and the vessel wall, were measured for at least four microspheres in each of the two data sets obtained from each vessel considered. Data sets with fewer than four microsphere measurements were not analyzed. Measurements were restricted to a section of vessel less than 15 μm in axial length. Measurements were not included if rolling or firmly adherent leukocytes were present in the 15-μm measurement window.

Since not all of the recorded beads travel in the midsagittal plane, only the fastest beads at a given measured radial location were considered (where it is understood that a bead in the midsagittal plane travels faster than any other bead at that measured radial location). If two beads were observed to travel at the same projection of their radial location (at two distinct times), only the faster bead would be used in the regression analysis, since it is assumed that the slower bead is traveling somewhat farther from the midsagittal plane than the faster bead and, therefore, would actually be at a greater radial distance from the vessel centerline. Furthermore, since the velocity distribution is known to be monotonically increasing with increasing distance from the wall, all beads should be ordered such that the bead farthest from the endothelium is traveling fastest with progressively closer beads traveling progressively slower. Any bead that did not satisfy this criterion was not included in the regression analysis.

For each vessel, μ-PIV data were used to estimate the thickness, t, of the ESL over a range of values of hydraulic resistivity, K. We regard the parameters t and K as being representative of the average properties of an ESL that likely varies axially in thickness and axially and radially in hydraulic resistivity, K. If these quantities are represented by their mean values, then this idealization is nevertheless quantitatively useful since it follows, from the mean-value theorem for integrals of continuous functions, that these quantities are bounded by the largest and smallest values they would assume in a heterogeneous, spatially nonuniform ESL. Henceforth, it will be implied that t and K denote the *effective* hydrodynamically relevant thickness and *effective* hydraulic resistivity, respectively.

Since the microspheres themselves influence near-wall microfluidics, the μ-PIV data were used to infer the translational speeds of fluid particles in the plasma-rich layer if no microspheres were present in the flow (Goldman et al., 1967). This was done iteratively to find t in each vessel for each fixed value of K that we considered. Beginning with the limiting case of no plasma flow through the ESL (i.e., in the limit as $K \to \infty$), a linear regression analysis was performed on the μ-PIV data in the plasma-rich region of a given vessel, which consistently extrapolated to a negative intercept at the vessel wall in every vessel that we observed. The distance from the vessel wall where the linear regression extrapolated to zero velocity was taken as our initial guess of the ESL thickness. Assuming a uniform shear field throughout the

plasma-rich region of the vessel and neglecting vessel curvature and any flow through the layer, the analysis of Goldman et al. was used to infer the translational speed a fluid particle would have, located a distance $h - t$ from the ESL interface, if the sphere, centered a distance $h - t$ from the interface, were not present in the flow. This was done for each sphere in the plasma-rich region of the vessel and a linear regression analysis was then performed on the predicted fluid-particle speeds. The distance from the vessel wall where this linear regression extrapolated to zero velocity was then taken as our updated guess of the ESL thickness. Fluid-particle speeds were then recomputed on the basis of this new layer thickness. Iteration continued until convergence on the precise layer thickness, t, was achieved.

A similar process was repeated for finite values of K in order of decreasing K starting with the largest finite value considered (10^{10} dyn-s/cm^4). For each finite value of K, iteration started with our estimate of t from the previous larger value of K. Approximating the layer as a Brinkman medium, and again assuming a uniform shear field throughout the plasma-rich region of the vessel and neglecting vessel curvature, the translational speed a fluid particle located a distance $h - t$ from the ESL interface, was inferred if the sphere, centered a distance $h - t$ from the interface, were not present in the flow (Damiano et al., 2003). Linear regression analysis of the fluid-particle speeds was used to find the slip velocity at the current estimate of the ESL interface. This slip velocity was then compared with the slip velocity predicted in the absence of spheres (Damiano et al., 1996). Successive updated thickness estimates were made by progressively increasing the current estimate until the value of t was obtained that corresponded to continuous velocity and shear-rate profiles across the interface. This procedure was repeated for several finite values of K (10^8, 10^9, and 10^{10} dyn-s/cm^4).

To make use of the analysis of Damiano et al. (1996) to perform the above-mentioned calculations, it is necessary to estimate the axial pressure-gradient component, dp/dz, since the slip velocity at the ESL interface scales linearly with dp/dz (Damiano et al., 1996). To make this estimate, we assume that the flow in the vessel is steady, axisymmetric, and fully developed and that in these microvessels the blood can be approximated as an incompressible, linearly viscous continuous fluid with a radially varying viscosity distribution over the vessel cross section (Cokelet, 1999). It is then evident from the conservation of linear momentum that even if the viscosity varies radially over the vessel cross section, the stress divergence and axial pressure-gradient component must both be constant and equal, and therefore the local shear stress must vary linearly with radial position, just as with a Poiseuille flow in a tube. In cylindrical coordinates (r, θ, z), the radial momentum equation can be integrated once with respect to radial position, r, under these assumptions to provide

$$\tau_{rz} = \mu(r)\frac{dv_z}{dr} = \frac{r}{2}\frac{dp}{dz}, \quad 0 \le r \le a, \tag{4}$$

where τ_{rz} is the local shear stress in the vessel, v_z is the axial velocity component, $\mu(r)$ is the local viscosity in the vessel, and $a = R - t$ corresponds to the radial location of the effective hydrodynamic interface of the ESL. If we impose the boundary condition that the local viscosity at the ESL interface is equal to plasma viscosity, μ_p, then we can solve Eq. 4 for dp/dz and evaluate it at $r = a$ to find

$$\frac{dp}{dz} = \frac{2\mu_p}{a}\frac{dv_z}{dr}\bigg|_{r=a} = \frac{2\mu_p}{a}\dot{\gamma}, \tag{5}$$

where $\dot{\gamma}$, subsequently referred to as the interfacial shear rate, is the shear rate evaluated at the effective hydrodynamic interface of the ESL. Over the course of converging upon the estimated ESL thickness for a particular data set, the current estimate of the radial location, a, of the ESL interface is known as is the current estimate of the interfacial shear rate, $\dot{\gamma}$, at every step in the iterative procedure described above for the case of a finite value of K. Therefore, an estimate of dp/dz can be made at each iteration using Eq. 5, which in turn allows us to infer the interfacial slip velocity at each iteration using the analysis of Damiano et al. (1996).

Statistical analysis

Data were expressed as mean ± SE Statistical significance between groups was determined using a two-tailed t-test with $p = 0.05$.

RESULTS

Optical artifacts

Consistent determination of the relative location of the anatomical vessel wall is essential to ensure accuracy of near-wall microsphere measurements (Gretz and Duling, 1995). Brightfield diameter measurements were validated by measurements, under fluorescence illumination, in cremaster muscle capillaries and venules of transgenic Tie2-GFP mice (39 vessels, 3–34 μm diameter). The Tie2 promoter-driven expression of GFP was found in endothelial cells only. All fluorescent diameter measurements were made using vessels for which both walls appeared bright. GFP fluorescent diameter is shown versus brightfield diameter in Fig. 1 *A*. The slope of a linear fit having zero intercept through the data was not significantly different from unity. The root mean-square absolute deviation in the difference between brightfield and GFP fluorescent diameters was 0.29 μm. In addition, FITC-dx fluorescent diameters were determined in capillaries and venules of WT mice before (31 vessels, 3.3–13 μm diameter) and after (22 vessels, 3.6–16 μm diameter) continuous epi-illumination to remove the ESL (Vink and Duling, 1996). Fig. 1 *B* shows that the width of the FITC-dx exclusion zone was significantly reduced after continuous epi-illumination (0.40 ± 0.05 μm before, 0.04 ± 0.03 μm after). This is consistent with previous results in hamster capillaries and small postcapillary venules (Vink and Duling, 1996; Henry and Duling, 1999) and larger than measurements in mouse cremaster capillaries (Platts et al., 2003).

To investigate the optical effects of a possible difference in the refractive indices of plasma and the surrounding tissue,

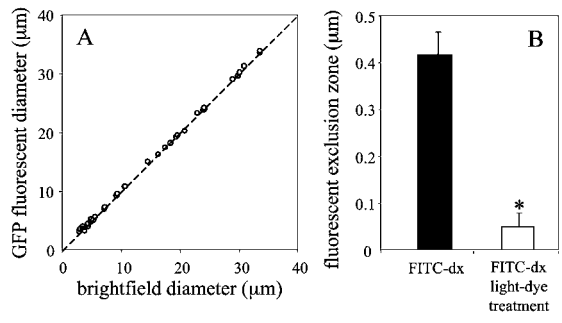

FIGURE 1 Brightfield diameter versus fluorescent diameter in capillaries and venules of Tie2 GFP transgenic mice (39 vessels, 3–34 μm diameter), which specifically express GFP in vascular endothelial cells (*A*). Line of unity shown (*dashed line*). FITC-dx fluorescent exclusion zone (one-half the difference in brightfield and fluorescent diameters) in capillaries and venules (*B*) of control vessels (*black*, 31 vessels, 3.3–13 μm diameter, in two WT mice) and vessels after continuous epi-illumination (*white*, 22 vessels, 3.6–16 μm diameter, in two WT mice). Asterisk denotes significant difference via two-tailed t-test ($p < 0.05$).

radially and axially aligned erythrocytes were measured in venules between 10 and 14 μm in diameter after occlusion of the vessel with a blunt micropipette. Fig. 2 *A* shows a photomicrograph of an axially aligned erythrocyte with its symmetry axis perpendicular to the vessel axis but parallel with the microscope's focal plane. Fig. 2 *B* shows a radially aligned erythrocyte aligned with its symmetry axis parallel to the vessel axis and parallel to the focal plane. Radially aligned erythrocytes were chosen for which transmitted light struck the vessel wall on a path toward the microscope at an angle $<90°$, assuming a circular vessel cross section. A significant difference in the refractive index of plasma and surrounding tissue should result in an underestimate of the width of radially aligned erythrocytes. Erythrocyte widths were 5.73 ± 0.11 μm and 5.61 ± 0.10 μm for radially or axially aligned cells, respectively, and the difference in these results was not statistically significant (Fig. 2 *C*; 45 radial and 45 axial erythrocytes in eight venules). These experiments were also performed with erythrocytes perfused through glass capillaries where there was a known difference in the refractive indices of the perfusion solution (plasma, $ND_p = 1.338$) and the bounding surface (glass, $ND_g = 1.48$). Photomicrographs of radially and axially aligned erythrocytes are shown in Fig. 2, *D* and *E*, respectively. Erythrocyte widths were 5.34 ± 0.07 μm and 5.92 ± 0.06 μm for radially or axially aligned cells, respectively, and the difference in these results was statistically significant (Fig. 2 *F*; 30 radial and 30 axial erythrocytes). Radially aligned erythrocytes of mean observed diameter 5.3 μm measured on average 4.5 μm from the capillary wall are predicted by Snell's law (Eq. 2) to have an actual erythrocyte length of 5.94 μm, which is in excellent agreement with the measurements of the lengths of axially aligned erythrocytes. It is noteworthy that the edge of a radially aligned 5.7-μm diameter erythrocyte in a 10–14-μm diameter vessel could be at most $\sim$2.2–4.2 μm from the endothelium, but were typically found to be much closer. This is consistent with the range of distances considered in the glass-tube experiments and thus the geometric factors that lead to optical artifacts in both the in vivo and in vitro experiments were comparable. Thus, the optical artifact measurements were made in the same region of the vessels in which microsphere data were obtained for μ-PIV. We therefore conclude that the difference in refractive indices between plasma and the surrounding tissue produces a negligibly small optical artifact.

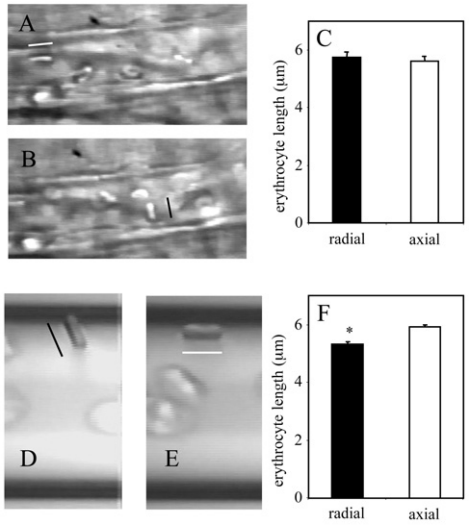

FIGURE 2 Photomicrographs showing axially (*A*, *white line*) or radially aligned erythrocytes (B, *black line*) in a 10.3 μm venule after occlusion with a blunt micropipette (micropipette not shown). Measurements of the diameter (width) of radially (*black*, 45 cells in eight venules) and axially aligned (*white*, 45 cells in eight venules) erythrocytes in 10–14 μm diameter venules (*C*). Photomicrographs showing radially (*D*, *black line*) or axially aligned erythrocytes (*E*, *white line*) in a 32 μm glass capillary after perfusion with a 2.5% hematocrit solution of mouse erythrocytes in plasma. Measurements of the diameter of radially (*black*, 30 cells) and axially aligned (*white*, 30 cells) erythrocytes (*F*). Asterisk denotes significant difference via two-tailed *t*-test ($p < 0.05$).

Estimated thickness of endothelial surface layer

Fluorescent microspheres were visualized flowing in close proximity to the endothelium in vivo. Over a 15-μm length of each vessel, two sets of μ-PIV data in the plasma-rich region near the vessel wall were analyzed (one set at $\theta = 0$ and another at $\theta = \pi$). Data sets containing fewer than four microsphere measurements were not used. From the analysis of 10 control vessels and 10 vessels after light-dye treatment, 34 total data sets were analyzed (17 in each group). The criterion that filtered μ-PIV data sets contain only microspheres having monotonically increasing velocities with increasing distance from the endothelium resulted in the removal of 59 out of a total of 121 microsphere measurements in control vessels and 43 out of a total of 104 microsphere measurements in light-dye treated vessels.

A photomicrograph of the double stroboscopic image of a single microsphere in a 21 μm diameter venule is shown in Fig. 3 *A*, where the black and white arrows point to the first and second images of the microsphere, respectively. The

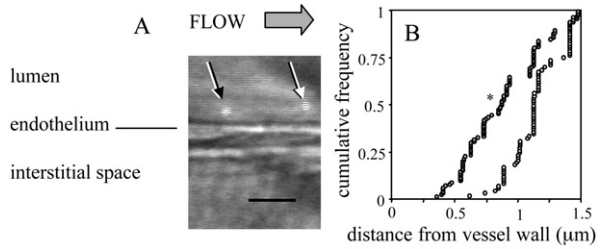

FIGURE 3 Photomicrograph of the double stroboscopic image of a single microsphere in a 21 μm diameter venule, where the black and white arrows point to the first and second images of the microsphere, respectively. Scale bar = 2 μm (*A*). Cumulative frequency of microspheres measured in close proximity to the vessel wall in control venules (*open circles*) and after prolonged exposure to epifluorescence treatment (*filled circles*, *B*). Asterisk denotes significant difference via two-tailed *t*-test ($p < 0.05$).

median distance of all microspheres in the near-wall zone (1.5 μm from the endothelial surface) was 1.14 μm in control vessels and 0.88 μm in light-dye treated vessels (Fig. 3 *B*). Thus, the median in the radial distribution of microspheres was 0.26 μm closer to the vessel wall in light-dye treated vessels than in control vessels. Using a two-tailed *t*-test ($p < 0.05$; Fig. 3 *B*), this difference in the distribution of radial positions between these two groups was found to be statistically significant.

Our estimates of the effective, hemodynamically relevant layer thickness, *t*, in one control vessel (Fig. 4, *A* and *C*) and one vessel after light-dye treatment (Fig. 4, *B* and *D*) are shown in Fig. 4. These estimates were obtained for the case of no flow through the ESL (i.e., in the limit as $K \rightarrow \infty$; Fig. 4, *A* and *B*) and for a hydraulic resistivity of $K = 10^8$ dyn-s/cm^4 (Fig. 4, *C* and *D*). The vertical asymptotes of the curves in Fig. 4, *E* and *F*, intersect the abscissa at values of h_a/a corresponding to when the microsphere just touches the glycocalyx interface in the control vessel and the light-dye treated vessel, respectively. The position of these asymptotes for the case of no flow through the layer (*solid curve* asymptotes: $h_a/a = 2.66$ in *E* and $h_a/a = 1.54$ in *F*) is therefore related to our estimate of the minimum dimensionless layer thickness in these two vessels according to $t/a = h_a/a - 1$ ($t = 0.39$ μm in *E* and $t = 0.13$ μm in *F*). The mean and standard error was determined in this way for 10 control venules (24–41 μm diameter) and 10 venules (18–31 μm diameter) after light-dye treatment to degrade the ESL, as shown in Fig. 5 for three finite values of *K* and in the limit as $K \rightarrow \infty$. Since these measurements were made on each of the two endothelial boundaries appearing in the two-dimensional projection of the midsagittal plane of a vessel, 10 control venules and 10 venules after light-dye treatment correspond to 40 total data sets. As expected, estimated mean effective layer thickness, $\bar{t}$, increased slightly with decreasing *K* ranging from a minimum, assuming no flow through the layer, of $\bar{t} \sim 0.33 \pm 0.04$ μm to a maximum of $\sim 0.44 \pm 0.04$ μm for $K = 10^8$ dyn-s/cm^4 in control vessels and from $\sim 0.07 \pm 0.02$ μm to $\sim 0.14 \pm 0.02$ μm in vessels after light-dye treatment to degrade the layer. Thus, continuous exposure of FITC-dx-filled vessels to epi-illumination results in a significant degradation of the layer by $\sim$75%.

Error analysis

The monotonic filter of the μ-PIV data described above had little impact on the final estimate of mean ESL thickness in control and light-dye treated vessels. The mean ESL thickness estimates in all control vessels (10 vessels, 17 total data sets) and all vessels after light-dye treatment (10 vessels, 17 total data sets) assuming infinite hydraulic resistivity after imposing the monotonicity requirement were $\bar{t} = 0.31 \pm$

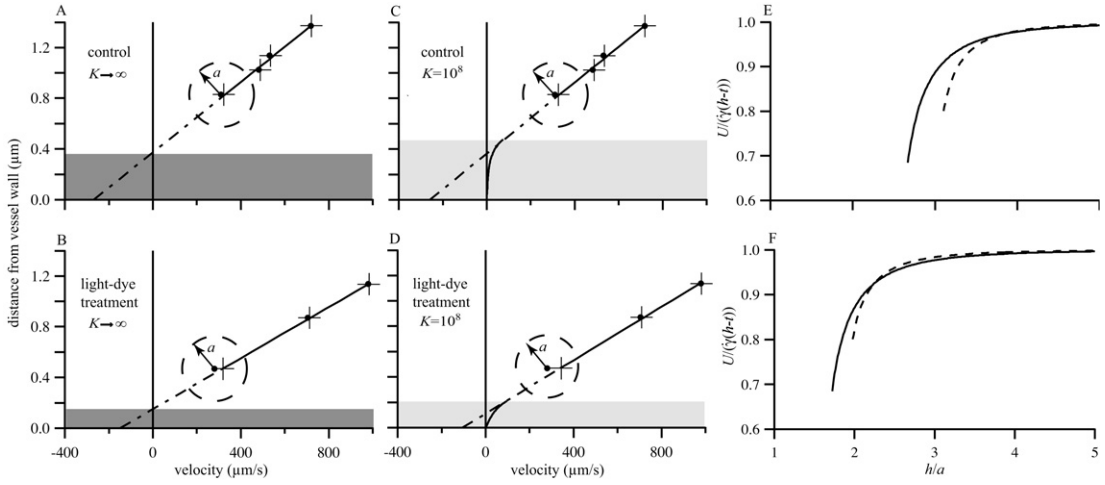

FIGURE 4 Fluorescent intravital μ-PIV data in the plasma-rich region of mouse cremaster muscle venules from one control vessel (*A* and *C*, 32.8 μm diameter) and a different vessel (*B* and *D*, 25.4 μm diameter) after light-dye treatment to degrade the ESL showing measured (*dot symbols*) translational speeds of sphere centers and predicted translational speeds of fluid-particles (*plus symbols*) if the spheres were not present in the flow. Theoretical curves in *E* and *F* are from an analysis of the free motion of a neutrally buoyant sphere in a uniform shear flow near a Brinkman medium and were used to estimate, as a function of h/a, the translational speed, *U*, a sphere of radius *a* would have, centered a distance *h* from the vessel wall, relative to the speed a fluid particle would have at that distance in a uniform shear field of strength $\dot{\gamma}$ if no sphere were present in the flow (Damiano et al., 2003). Curves corresponding to $U/((h-t)\dot{\gamma})$ in *E* were used to relate sphere translational speeds in the control vessel to predicted fluid-particle speeds in *A* assuming no flow through the layer (*solid curve*, $K \rightarrow \infty$) and in *C* assuming a finite hydraulic resistivity (*dashed*, $K = 10^8$ dyn-s/cm^4). The curves in *F* are similarly related to *B* and *D* in the light-dye treated vessel. In every vessel we observed, linear extrapolation (*dash-dotted line* in *A–D*) of the linear fit to the estimated fluid-particle velocity data revealed a negative intercept at the vessel wall. Permeation-induced fluid drag through the glycocalyx is thought to account for the enhanced drag on the portion of the microsphere that is nearest to the glycocalyx interface. When flow through the ESL is neglected, as in *A* and *B*, layer thickness, *t*, is estimated as the distance from the vessel wall where the linear fit extrapolates to zero velocity, whereas for finite values of *K*, as in *C* and *D*, layer thickness is estimated using predicted velocity profiles in the layer (Damiano et al., 1996) as described in Materials and Methods.

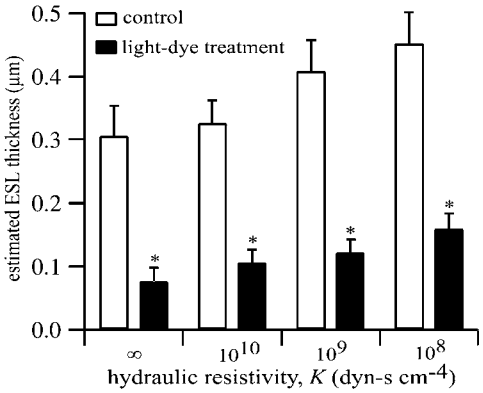

FIGURE 5 Mean layer thickness of control vessels (*white*, 10 vessels, 24–41 μm diameter, in four WT mice) and of light-dye treated vessels (*black*, 10 vessels, 18–31 μm diameter, in three WT mice) obtained from the average of individual estimates of t found (as in Fig. 4) for three finite values of hydraulic resistivity ($K = 10^8$, 10^9, and 10^{10} dyn-s/cm^4) and for the case of no flow through the layer ($K \rightarrow \infty$). Asterisk denotes significant difference via two-tailed t-test ($p < 0.05$).

0.04 μm and $\bar{t} = 0.08 \pm 0.02$ μm, respectively. This value differed little from the mean ESL thickness using all data without imposing the monotonic filter ($\bar{t} = 0.33 \pm 0.05$ μm in control and $\bar{t} = 0.07 \pm 0.02$ μm in light-dye treated vessels).

DISCUSSION

Using high-resolution near-wall μ-PIV, our results provide direct evidence for a hemodynamically relevant ESL in microvessels in vivo. A substantial change in ESL thickness after light-dye treatment is the most reasonable explanation that could account for the change in the radial distribution of microspheres within 1.5 μm of the wall and the change in the fluid velocity distribution throughout the plasma layer. We emphasize that all of our measurements of microsphere position are consistently referenced to the same position on the membrane before and after light-dye treatment (see Materials and Methods). Although there may be some ambiguity as to how that reference might be chosen, and therefore in the precise thickness of the ESL in an absolute sense, the change in thickness after light-dye treatment can be accurately estimated with confidence. Since the change in thickness must be less than, or at most equal to, the absolute thickness of the intact ESL in control vessels, we regard our estimates of the change in thickness of the ESL as lower bounds on the true absolute thickness of the ESL in vivo.

Confirmation of the existence and apparent in vivo thickness of an ESL, first estimated based on dye and erythrocyte exclusion techniques in capillaries and small postcapillary venules (Vink and Duling, 1996; Henry and Duling, 1999; Vink and Duling, 2000; Henry and Duling, 2000), and by an indirect method based on hemodynamic modeling calculations in microvascular networks (Pries et al., 1997), and now by a third, direct, and completely independent method using intravital μ-PIV in venules, offers increasing confidence in the true extent of this structure in vivo over and against earlier estimates inferred from electron microscopy studies. Since microspheres are not likely to significantly invade the ESL, the upper bound on our estimate of layer thickness, t_{max}, in a given venule is determined by the clearance, $h - a$, of the nearest microspheres to the vessel wall. This in turn places a lower bound on the hydraulic resistivity, which we estimate to be $K > \sim 10^8$ dyn-s/cm^4 since, in most of the vessels we observed, significantly lower values of K would have required a layer thickness in excess of t_{max}. For the range of values of K considered, our results (see Fig. 5) show little sensitivity in estimated layer thickness on the precise value of K (layer thickness estimate varies only $\sim$33% for $\infty > K > 10^8$ dyn-s/cm^4). This is a consequence of the considerable retardation of plasma flow through the layer over this range of K (see Fig. 4, C and D).

Whereas numerous theoretical models have been developed that clearly suggest that an ESL with substantial hydraulic resistivity has important implications in broad areas of microvascular physiology (Damiano et al., 1996, 1998b; Secomb et al., 1998; Feng and Weinbaum, 2000; Damiano and Stace, 2002), very little direct experimental evidence exists that confirms this hypothesis. Using numerical simulations of blood flow through microvascular networks, Pries and coworkers found that blood flow measurements in microvessels in vivo were indicative of an elevated apparent viscosity relative to blood flow through glass tubes of similar diameter (Pries et al., 1990, 1994). A later investigation found a 14–21% decrease in flow resistance of blood through microvessels in vivo after microinjection of heparinase (Pries et al., 1997). Reinhart et al. (1993) found that the terminal velocity of $\sim$175-μm-diameter microspheres coated with confluent porcine aortic endothelial cells falling through plasma was reduced compared to cell culture media, suggesting the ESL has increased hydraulic resistivity in plasma. The μ-PIV data presented here are the most direct demonstration to date that the ESL retards plasma flow. An ESL with these properties has significant implications for microvascular physiology (Pries et al., 2000).

First, any molecule present in the vessel lumen will have to negotiate a very thick, largely unstirred surface layer far beyond the distances conventionally assumed (Renkin, 1994; Hu and Weinbaum, 1999). Second, these findings have important implications for near-wall microfluidics and stress transmission to vascular endothelium. Based on our μ-PIV data, we conclude that retardation of plasma by the layer must be so great that the fluid shear rate (and hence fluid shear stress) on the endothelial-cell surface is effectively zero (see Fig. 4, C and D). Recent studies have made similar predictions on purely theoretical grounds (Damiano et al., 1996; Damiano, 1998b; Secomb et al., 1998, 2001a); however, this is the first in vivo evidence based on direct experimental evidence of local microfluidics. The implications of

these findings are that nearly all of the mechanical stress from the blood flowing in the vessel lumen is transferred to the macromolecular matrix of the glycocalyx in the form of tension in its macromolecular constituents. The transmission of mechanical stress from the fluid flow in the lumen to the endothelial-cell cytoskeleton is likely to occur through the transfer of stress from fluid flow through the glycocalyx near its apical end to the transmembrane domains of proteoglycans near the base of the layer. The endothelial-cell lipid bilayer, on the other hand, bears very little stress from the prevailing flow in the vessel, as most of this stress is communicated from the ESL directly to the endothelial-cell cytoskeleton.Third, although its implications for microvascular rheology are most profound in capillaries, a 0.5-μm-thick ESL, having relatively low hydraulic permeability, would also exert a significant influence on microvascular rheology in vessels as large as 50 μm in diameter. Assuming Poiseuille flow in the vessel as a first approximation, the removal of a 0.5-μm-thick ESL that completely retards plasma flow (i.e., in the limit as $K \rightarrow \infty$) would result in a decrease in flow resistance by 14% and 8% in venules 30 and 50 μm in diameter, respectively. However, because of the Fahraeus-Lindqvist effect, apparent viscosity increases with increasing vessel diameter over this range so that removal of the ESL would result in a greater decrease in flow resistance than would be predicted by the fourth power dependence on tube diameter given by Poiseuille's law (Damiano, 1998a).

Finally, it is likely that the ESL modulates the inflammatory response. Rolling leukocytes attach to blood vessel walls using molecules that extend 20–50 nm above the plasma membrane (Springer, 1995). Based on current estimates of the hydraulic resistivity and restoring forces of the layer (Zhao et al., 2001; Feng and Weinbaum, 2000; Damiano and Stace, 2002; Secomb et al., 2001b), the stiffness of the leukocyte microvilli is insufficient to penetrate a surface layer, making de novo attachment of leukocytes from the free stream (''primary capture'') a rare event. Indeed, experimental evidence shows that primary capture is exceedingly rare in inflamed small microvessels (Kunkel et al., 1998). When free-flowing leukocytes attach to the walls of larger venules (>45 μm diameter), which is also a rare event, this occurs mainly through leukocyte-leukocyte interactions (''secondary capture'') (Eriksson et al., 2001). However, the vast majority of rolling leukocytes attach at the entrance of postcapillary venules (Schmid-Schoenbein et al., 1980; Dunne et al., 2002), where deformed leukocytes exit from capillaries with a diameter smaller than the resting leukocyte diameter. It is possible that, under these conditions, the leukocyte membrane is squeezed tightly enough against the wall so that initial bonds can form between the leukocyte and the endothelium. Previous work has shown that the ESL in capillaries is highly compressed by passing leukocytes (Vink and Duling, 1996). Once a bond has been established between leukocytes and endothelial cells, it is easy to envision how tension in the selectin bond would be sufficient to overwhelm restoring forces in the glycocalyx and keep the leukocyte in close enough proximity to the endothelium to support selectin-mediated rolling. In addition, the ESL may significantly change its properties under inflammatory conditions (Henry and Duling, 2000; Vink et al., 2000; Mulivor and Lipowsky, 2002; Platts et al., 2003), which may facilitate sustained rolling and adhesion of leukocytes.

The method presented here could be used to elucidate the significance of the ESL in inflammatory states. Considering the possibility that the ESL is ''shed'' from endothelial cells after severe inflammatory insults (Henry and Duling, 2000; Key et al., 1992) and that the stiffness of leukocyte microvilli is insufficient to penetrate the ESL (Zhao et al., 2001), leukocyte rolling may be dependent on ESL thickness. Variability in rolling flux fraction between different venules after addition of TNF-α, for instance, may be due in part to differences in the thickness or mechanical properties of the residual ESL. In addition, variability in the rolling velocity of leukocytes along the length of a venule could be due to variability in the thickness of the ESL.

The present study does not address the molecular nature of the ESL, but rather reveals the hemodynamic consequences of this layer. The direct confirmation of a hemodynamically relevant ESL emphasizes the necessity to revise previous concepts of wall shear rate, wall shear stress, leukocyte adhesion, microvascular flow resistance, stress transmission to vascular endothelium, and endothelial mechanotransduction mechanisms.

We thank Michele Kirkpatrick for animal husbandry. Tie2-GFP mice were a kind gift of Dr. Joel Linden. Glass capillaries were a kind gift of Dr. Axel Pries.

This work was supported by National Institutes of Health grant HL64381 to K.L. and the Whitaker Foundation (RG-98-0524 to E.R.D.). M.L.S. supported by National Institutes of Health grant T32 GM 08715-01A1 to Gordon Laurie and K.L.

REFERENCES

Baez, S. 1973. An open cremaster muscle preparation for the study of blood vessels by in vivo microscopy. *Microvasc. Res.* 5:384–394.

Cokelet, G. R. 1999. Viscometric, in vitro and in vivo blood viscosity relationships: how are they related? *Biorheology.* 36:343–358.

Damiano, E. R. 1998a. Blood flow in microvessels lined with a poroelastic wall layer. *In* Poromechanics. J.-F. Thimus, Y. Abousleiman, A. H. D. Cheng, O. Coussy, and E. Detournay, editors. Balkema, Rotterdam, The Netherlands. 403–408.

Damiano, E. R. 1998b. The effect of the endothelial-cell glycocalyx on the motion of red blood cells through capillaries. *Microvasc. Res.* 55:77–91.

Damiano, E. R., B. R. Duling, K. Ley, and T. C. Skalak. 1996. Axisymmetric pressure-driven flow of rigid pellets through a cylindrical tube lined with a deformable porous wall layer. *J. Fluid Mech.* 314:163–189.

Damiano, E. R., D. S. Long, F. H. El-Khatib, and T. M. Stace. 2003. On the motion of a sphere in a Stokes flow parallel to a Brinkman half space. *J. Fluid Mech.* In press.

Damiano, E. R., and T. M. Stace. 2002. A mechano-electrochemical model of radial deformation of the capillary glycocalyx. *Biophys. J.* 82:1153–1175.

Desjardins, C., and B. R. Duling. 1990. Heparinase treatment suggests a role for the endothelial cell glycocalyx in regulation of capillary hematocrit. *Am. J. Physiol.* 258:H647–H654.

Dunne, J. L., C. M. Ballantyne, A. L. Beaudet, and K. Ley. 2002. Control of leukocyte rolling velocity in TNF-α-induced inflammation by LFA-1 and Mac-1. *Blood.* 99:336–341.

Eriksson, E. E., X. Xie, J. Werr, P. Thoren, and L. Lindbom. 2001. Importance of primary capture and L-selectin-dependent secondary capture in leukocyte accumulation in inflammation and atherosclerosis in vivo. *J. Exp. Med.* 194:205–218.

Feng, J., and S. Weinbaum. 2000. Lubrication theory in highly compressible porous media: the mechanics of skiing, from red cells to humans. *J. Fluid Mech.* 422:281–317.

Goldman, A. J., R. G. Cox, and H. Brenner. 1967. Slow viscous motion of a sphere parallel to a plane wall—II Couette flow. *Chem. Eng. Sci.* 22:653–660.

Gretz, J. E., and B. R. Duling. 1995. Measurement uncertainties associated with the use of bright-field and fluorescence microscopy in the microcirculation. *Microvasc. Res.* 49:134–140.

Haldenby, K. A., D. C. Chappell, C. P. Winlove, K. H. Parker, and J. A. Firth. 1994. Focal and regional variations in the composition of the glycocalyx of large vessel endothelium. *J. Vasc. Res.* 31:2–9.

Henry, C. B., and B. R. Duling. 1999. Permeation of the luminal capillary glycocalyx is determined by hyaluronan. *Am. J. Physiol.* 277:H508–H514.

Henry, C. B., and B. R. Duling. 2000. TNF-α increases entry of macromolecules into luminal endothelial cell glycocalyx. *Am. J. Physiol.* 279:H2815–H2823.

Hu, X., and S. Weinbaum. 1999. A new view of Starling's hypothesis at the microstructural level. *Microvasc. Res.* 58:281–304.

Inoue, S. 1986. Microscope Image Formation. *In* Video Microscopy. S. Inoue, editor. Plenum Press, New York. 93–148.

Key, N. S., J. L. Platt, and G. M. Vercellotti. 1992. Vascular endothelial cell proteoglycans are susceptible to cleavage by neutrophils. *Arterioscler. Thromb.* 12:836–842.

Kunkel, E. J., J. E. Chomas, and K. Ley. 1998. Role of primary and secondary capture for leukocyte accumulation in vivo. *Circ. Res.* 82:30–38.

Ley, K., D. C. Bullard, M. L. Arbones, R. Bosse, D. Vestweber, T. F. Tedder, and A. L. Beaudet. 1995. Sequential contribution of L- and P-selectin to leukocyte rolling in vivo. *J. Exp. Med.* 181:669–675.

Motoike, T., S. Loughna, E. Perens, B. L. Roman, W. Liao, T. C. Chau, C. D. Richardson, T. Kawate, J. Kuno, B. M. Weinstein, D. Y. Stainier, and T. N. Sato. 2000. Universal GFP reporter for the study of vascular development. *Genesis.* 28:75–81.

Mulivor, A. W., and H. H. Lipowsky. 2002. Role of glycocalyx in leukocyte-endothelial cell adhesion. *Am. J. Physiol.* 283:H1282–H1291.

Norman, K. E. 2001. An effective and economical solution for digitizing and analyzing video recordings of the microcirculation. *Microcirculation.* 8:243–249.

Platts, S. H., J. Linden, and B. R. Duling. 2003. Rapid modification of the glycocalyx caused by ischemia/reperfusion is inhibited by adenosine A2A receptor activation. *Am. J. Physiol.* 284:H2364–H2367.

Pries, A. R., T. W. Secomb, and P. Gaehtgens. 2000. The endothelial surface layer. *Pflugers Arch.* 440:653–666.

Pries, A. R., T. W. Secomb, P. Gaehtgens, and J. F. Gross. 1990. Blood flow in microvascular networks. Experiments and simulation. *Circ. Res.* 67:826–834.

Pries, A. R., T. W. Secomb, T. Gessner, M. B. Sperandio, J. F. Gross, and P. Gaehtgens. 1994. Resistance to blood flow in microvessels in vivo. *Circ. Res.* 75:904–915.

Pries, A. R., T. W. Secomb, H. Jacobs, M. Sperandio, K. Osterloh, and P. Gaehtgens. 1997. Microvascular blood flow resistance: role of endothelial surface layer. *Am. J. Physiol.* 273:H2272–H2279.

Reinhart, W. H., C. M. Boulanger, T. F. Luscher, A. Haeberli, and P. W. Straub. 1993. Influence of endothelial surface on flow velocity in vitro. *Am. J. Physiol.* 265:H523–H529.

Reinke, W., P. Gaehtgens, and P. C. Johnson. 1987. Blood viscosity in small tubes: effect of shear rate, aggregation, and sedimentation. *Am. J. Physiol.* 253:H540–H547.

Renkin, E. M. 1994. Cellular aspects of transvascular exchange: a 40-year perspective. *Microcirculation.* 1:157–167.

Schmid-Schoenbein, G. W., S. Usami, R. Skalak, and S. Chien. 1980. The interaction of leukocytes and erythrocytes in capillary and postcapillary vessels. *Microvasc. Res.* 19:45–70.

Secomb, T. W., R. Hsu, and A. R. Pries. 1998. A model for red blood cell motion in glycocalyx-lined capillaries. *Am. J. Physiol.* 274:H1016–H1022.

Secomb, T. W., R. Hsu, and A. R. Pries. 2001a. Effect of the endothelial surface layer on transmission of fluid shear stress to endothelial cells. *Biorheology.* 38:143–150.

Secomb, T. W., R. Hsu, and A. R. Pries. 2001b. Motion of red blood cells in a capillary with an endothelial surface layer: effect of flow velocity. *Am. J. Physiol.* 281:H629–H636.

Sims, D. E., and M. M. Horne. 1994. Non-aqueous fixative preserves macromolecules on the endothelial cell surface: an in situ study. *Eur. J. Morphol.* 32:59–64.

Springer, T. A. 1995. Traffic signals on endothelium for lymphocyte recirculation and leukocyte emigration. *Annu. Rev. Physiol.* 57:827–872.

Stace, T. M., and E. R. Damiano. 2001. An electrochemical model of the transport of charged molecules through the capillary glycocalyx. *Biophys. J.* 80:1670–1690.

Vink, H., A. A. Constantinescu, and J. A. Spaan. 2000. Oxidized lipoproteins degrade the endothelial surface layer: implications for platelet-endothelial cell adhesion. *Circulation.* 101:1500–1502.

Vink, H., and B. R. Duling. 1996. Identification of distinct luminal domains for macromolecules, erythrocytes, and leukocytes within mammalian capillaries. *Circ. Res.* 79:581–589.

Vink, H., and B. R. Duling. 2000. Capillary endothelial surface layer selectively reduces plasma solute distribution volume. *Am. J. Physiol.* 278:H285–H289.

Zhao, Y., S. Chien, and S. Weinbaum. 2001. Dynamic contact forces on leukocyte microvilli and their penetration of the endothelial glycocalyx. *Biophys. J.* 80:1124–1140.